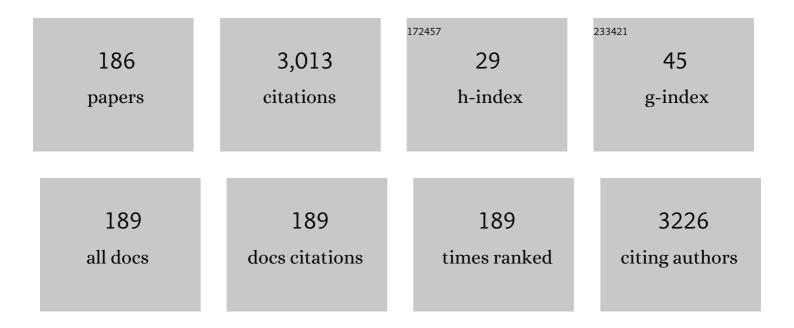
Zainovia Lockman

List of Publications by Year in descending order

Source: https://exaly.com/author-pdf/3130790/publications.pdf Version: 2024-02-01



#	Article	IF	CITATIONS
1	Structural and Morphology of ZnO Nanorods Synthesized Using ZnO Seeded Growth Hydrothermal Method and Its Properties as UV Sensing. PLoS ONE, 2012, 7, e50405.	2.5	121
2	Photoactivity of anatase–rutile TiO2 nanotubes formed by anodization method. Thin Solid Films, 2009, 518, 16-21.	1.8	115
3	Fabrication and Characterization of Glucose Biosensors by Using Hydrothermally Grown ZnO Nanorods. Scientific Reports, 2018, 8, 13722.	3.3	101
4	Size dependent ferromagnetism in cerium oxide (CeO ₂) nanostructures independent of oxygen vacancies. Journal of Physics Condensed Matter, 2008, 20, 165201.	1.8	97
5	Fast-rate formation of TiO ₂ nanotube arrays in an organic bath and their applications in photocatalysis. Nanotechnology, 2010, 21, 365603.	2.6	97
6	Influence of electrolyte pH on TiO2 nanotube formation by Ti anodization. Journal of Alloys and Compounds, 2009, 485, 478-483.	5.5	83
7	Influence of anodisation voltage on the dimension of titania nanotubes. Journal of Alloys and Compounds, 2010, 503, 359-364.	5.5	76
8	Electrochemical growth of ZnO nano-rods on polycrystalline Zn foil. Nanotechnology, 2003, 14, 968-973.	2.6	70
9	Extremely Fast Growth Rate of TiO2 Nanotube Arrays in Electrochemical Bath Containing H2O2. Journal of the Electrochemical Society, 2011, 158, C397.	2.9	70
10	Effect of applied voltage and fluoride ion content on the formation of zirconia nanotube arrays by anodic oxidation of zirconium. Corrosion Science, 2011, 53, 1156-1164.	6.6	70
11	Effects of Postdeposition Annealing in Argon Ambient on Metallorganic Decomposed CeO[sub 2] Gate Spin Coated on Silicon. Journal of the Electrochemical Society, 2010, 157, H6.	2.9	61
12	Elaboration and characterization of sol–gel derived ZrO2 thin films treated with hot water. Applied Surface Science, 2012, 258, 5250-5258.	6.1	59
13	Effects of the size and filler loading on the properties of copper―and silverâ€nanoparticleâ€filled epoxy composites. Journal of Applied Polymer Science, 2011, 121, 3145-3152.	2.6	51
14	Growth of strongly biaxially aligned MgB2 thin films on sapphire by postannealing of amorphous precursors. Applied Physics Letters, 2001, 79, 4001-4003.	3.3	40
15	Structure of the superconducting gap in MgB2from point-contact spectroscopy. Superconductor Science and Technology, 2002, 15, 526-532.	3.5	40
16	Methylene blue dye removal on silver nanoparticles reduced by Kyllinga brevifolia. Environmental Science and Pollution Research, 2019, 26, 11482-11495.	5.3	38
17	Oxidation of etched Zn foil for the formation of ZnO nanostructure. Journal of Alloys and Compounds, 2011, 509, 6806-6811.	5.5	37
18	Comparison of metal-organic decomposed (MOD) cerium oxide (CeO2) gate deposited on GaN and SiC substrates. Journal of Crystal Growth, 2011, 326, 2-8.	1.5	37

#	Article	IF	CITATIONS
19	Physical and Electrochemical Properties of Iron Oxide Nanoparticles-modified Electrode for Amperometric Glucose Detection. Electrochimica Acta, 2017, 248, 160-168.	5.2	36
20	Nanomaterial Fabrication through the Modification of Sol–Gel Derived Coatings. Nanomaterials, 2021, 11, 181.	4.1	36
21	Formation of self-aligned ZnO nanorods in aqueous solution. Journal of Alloys and Compounds, 2010, 493, 699-706.	5.5	35
22	Room temperature anodic deposition and shape control of one-dimensional nanostructured zinc oxide. Journal of Alloys and Compounds, 2009, 476, 513-518.	5.5	34
23	Electrical Properties of Pulsed Laser Deposited Y[sub 2]O[sub 3] Gate Oxide on 4H–SiC. Electrochemical and Solid-State Letters, 2010, 13, H396.	2.2	33
24	Ag nanoparticle-deposited TiO2 nanotube arrays for electrodes of Dye-sensitized solar cells. Nanoscale Research Letters, 2015, 10, 219.	5.7	33
25	Formation of highly crystallized ZnO nanostructures by hot-water treatment of etched Zn foils. Materials Letters, 2013, 91, 111-114.	2.6	32
26	Synthesis of freestanding amorphous ZrO 2 nanotubes by anodization and their application in photoreduction of Cr(VI) under visible light. Surface and Coatings Technology, 2017, 320, 371-376.	4.8	32
27	Effect of annealing on acid-treated WO 3 ·H 2 O nanoplates and their electrochromic properties. Electrochimica Acta, 2015, 178, 673-681.	5.2	30
28	Synthesis of rutile TiO2 nanowires by thermal oxidation of titanium in the presence of KOH and their ability to photoreduce Cr(VI) ions. Journal of Alloys and Compounds, 2020, 812, 152094.	5.5	30
29	Microwave surface resistance of MgB2. Applied Physics Letters, 2002, 80, 2347-2349.	3.3	29
30	The microwave surface impedance of MgB2thin films. Superconductor Science and Technology, 2003, 16, 1-6.	3.5	29
31	Effect of Postdeposition Annealing in Oxygen Ambient on Gallium-Nitride-Based MOS Capacitors With Cerium Oxide Gate. IEEE Transactions on Electron Devices, 2011, 58, 122-131.	3.0	29
32	Preparation of anodic nanoporous WO3 film using oxalic acid as electrolyte. Journal of Alloys and Compounds, 2017, 704, 518-527.	5.5	29
33	Fabrication of titanium-based alloys with bioactive surface oxide layer as biomedical implants: Opportunity and challenges. Transactions of Nonferrous Metals Society of China, 2022, 32, 1-44.	4.2	29
34	Photoluminescence properties of rod-like Ce-doped ZnO nanostructured films formed by hot-water treatment of sol–gel derived coating. Optical Materials, 2013, 35, 1902-1907.	3.6	28
35	The rapid growth of 3 µm long titania nanotubes by anodization of titanium in a neutral electrochemical bath. Nanotechnology, 2010, 21, 055601.	2.6	27
36	Oxidation of sputtered Zr thin film on Si substrate. Journal of Materials Science: Materials in Electronics, 2011, 22, 143-150.	2.2	27

#	Article	IF	CITATIONS
37	Effects of post-oxidation annealing temperature on ZrO2 thin film deposited on 4H-SiC substrate. Materials Science in Semiconductor Processing, 2011, 14, 13-17.	4.0	27
38	Physical characterization of post-deposition annealed metal-organic decomposed cerium oxide film spin-coated on 4H-silicon carbide. Journal of Alloys and Compounds, 2010, 497, 195-200.	5.5	26
39	Physical and electrical characteristics of metal-organic decomposed CeO2 gate spin-coated on 4H-SiC. Applied Physics A: Materials Science and Processing, 2011, 103, 1067-1075.	2.3	26
40	Investigation of forming-gas annealed CeO2 thin film on GaN. Journal of Materials Science: Materials in Electronics, 2011, 22, 583-591.	2.2	25
41	Effects of post-deposition annealing temperature and time on physical properties of metal-organic decomposed lanthanum cerium oxide thin film. Thin Solid Films, 2011, 519, 5139-5145.	1.8	24
42	WO3 nanorods prepared by low-temperature seeded growth hydrothermal reaction. Journal of Alloys and Compounds, 2014, 588, 585-591.	5.5	24
43	Electroless Deposition of Ferromagnetic Cobalt Nanoparticles in Propylene Glycol. Journal of the Electrochemical Society, 2009, 156, E139.	2.9	23
44	Effects of N2O Postdeposition Annealing on Metal-Organic Decomposed CeO2 Gate Oxide Spin-Coated on GaN Substrate. Journal of the Electrochemical Society, 2011, 158, H423.	2.9	23
45	TiO 2 nanotube arrays formation in fluoride/ethylene glycol electrolyte containing LiOH or KOH as photoanode for dye-sensitized solar cell. Journal of Photochemistry and Photobiology A: Chemistry, 2017, 343, 33-39.	3.9	23
46	Effect of ultrasonication medium on the properties of copper nanoparticle-filled epoxy composite for electrical conductive adhesive (ECA) application. Journal of Materials Science: Materials in Electronics, 2010, 21, 772-778.	2.2	22
47	Metal-oxide-semiconductor characteristics of lanthanum cerium oxide film on Si. Applied Physics A: Materials Science and Processing, 2012, 107, 459-467.	2.3	21
48	Sunlight activated anodic freestanding ZrO ₂ nanotube arrays for Cr(VI) photoreduction. Nanotechnology, 2018, 29, 375701.	2.6	21
49	Study of thermal oxidation of NiO buffers on Ni-based tapes for superconductor substrates. Physica C: Superconductivity and Its Applications, 2001, 351, 34-37.	1.2	20
50	Rapid Growth of Nd2â^'xCexCuO4 Thick Films as a Buffer for the Growth of Rare-earth Barium Cuprate–coated Conductors. Journal of Materials Research, 2002, 17, 1-4.	2.6	20
51	MOS Characteristics of Metallorganic-Decomposed CeO[sub 2] Spin-Coated on GaN. Electrochemical and Solid-State Letters, 2010, 13, H116.	2.2	20
52	Effects of Post-Deposition Annealing on CeO ₂ Gate Prepared by Metal-Organic Decomposition (MOD) Method on 4H-SiC. Materials Science Forum, 0, 645-648, 837-840.	0.3	20
53	Synthesis of ZnO nanorod–nanosheet composite via facile hydrothermal method and their photocatalytic activities under visible-light irradiation. Journal of Solid State Chemistry, 2014, 211, 146-153.	2.9	19
54	Effect of annealing temperature on anodized nanoporous WO3. Journal of Porous Materials, 2015, 22, 537-544.	2.6	19

#	Article	IF	CITATIONS
55	Rapid nanosheets and nanowires formation by thermal oxidation of iron in water vapour and their applications as Cr(VI) adsorbent. Applied Surface Science, 2016, 380, 172-177.	6.1	19
56	Initial growth study of TiO 2 nanotube arrays anodised in KOH/fluoride/ethylene glycol electrolyte. Materials and Design, 2017, 128, 195-205.	7.0	19
5 7	In situ mixed potential study of the growth of zinc oxide hierarchical nanostructures by wet oxidation of zinc foil. Journal of Materials Science, 2017, 52, 2319-2328.	3.7	19
58	Rapid formation of transparent CuAlO2 thin film by thermal annealing of Cu on Al2O3. Solar Energy Materials and Solar Cells, 2009, 93, 1383-1387.	6.2	18
59	Anodic Ag/TiO ₂ nanotube array formation in NaOH/fluoride/ethylene glycol electrolyte as a photoanode for dye-sensitized solar cells. Nanotechnology, 2016, 27, 355605.	2.6	18
60	Self-Assembled Iron Oxide Nanoparticle-Modified APTES-ITO Electrode for Simultaneous Stripping Analysis of Cd(II) and Pb(II) Ions. ACS Omega, 2022, 7, 3823-3833.	3.5	18
61	Photoelectrochemical Behaviour of Uniform Growth TiO ₂ Nanotubes via Bubble Blowing Synthesised in Ethylene Glycol with Hydrogen Peroxide. Journal of Nanoscience and Nanotechnology, 2012, 12, 4057-4066.	0.9	17
62	Immuno-probed graphene nanoplatelets on electrolyte-gated field-effect transistor for stable cortisol quantification in serum. Journal of the Taiwan Institute of Chemical Engineers, 2020, 117, 10-18.	5.3	17
63	Formation of ZnO nanorod arrays on polytetraflouroethylene (PTFE) via a seeded growth low temperature hydrothermal reaction. Journal of Alloys and Compounds, 2011, 509, 820-826.	5.5	16
64	Hexavalent Chromium Removal via Photoreduction by Sunlight on Titanium–Dioxide Nanotubes Formed by Anodization with a Fluorinated Glycerol–Water Electrolyte. Catalysts, 2021, 11, 376.	3.5	16
65	Improved current densities in MgB2 by liquid-assisted sintering. Applied Physics Letters, 2005, 86, 242501.	3.3	15
66	Stimulation of silicon carbide nanotubes formation using different ratios of carbon nanotubes to silicon dioxide nanopowders. Journal of Alloys and Compounds, 2009, 475, 565-568.	5.5	15
67	The Assessment of Cr(VI) Removal by Iron Oxide Nanosheets and Nanowires Synthesized by Thermal Oxidation of Iron in Water Vapour. Procedia Chemistry, 2016, 19, 586-593.	0.7	15
68	Hydrothermal synthesis of bismuth nanosheets for modified APTES-functionalized screen-printed carbon electrode in lead and cadmium detection. Journal of Nanoparticle Research, 2020, 22, 1.	1.9	15
69	The effect of oxygenation on the superconducting properties of MgB2 thin films. Applied Physics Letters, 2005, 86, 022502.	3.3	14
70	Effect of post-deposition annealing temperature on CeO2 thin film deposited on silicon substrate via RF magnetron sputtering technique. Materials Science in Semiconductor Processing, 2011, 14, 101-107.	4.0	14
71	Fabrication of well-crystallized mesoporous ZrO2 thin films via Pluronic P123 templated sol–gel route. Ceramics International, 2013, 39, S437-S440.	4.8	14
72	Blue-emitting photoluminescence of rod-like and needle-like ZnO nanostructures formed by hot-water treatment of sol–gel derived coatings. Journal of Luminescence, 2015, 158, 44-49.	3.1	14

#	Article	IF	CITATIONS
73	Comparison of ZrO2, TiO2, and α-Fe2O3 nanotube arrays on Cr(VI) photoreduction fabricated by anodization of Zr, Ti, and Fe foils. Materials Research Express, 2020, 7, 055013.	1.6	14
74	ITO electrode modified with Pt nanodendrites-decorated ZnO nanorods for enzymatic glucose sensor. Journal of Solid State Electrochemistry, 2021, 25, 1065-1072.	2.5	14
75	Study of thermal oxidation of NiO on pure Ni, Ni-10% Cr and Ni-9% V tapes. IEEE Transactions on Applied Superconductivity, 2001, 11, 3325-3328.	1.7	13
76	Design of hierarchically meso–macroporous tetragonal ZrO2 thin films with tunable thickness by spin-coating via sol–gel template route. Microporous and Mesoporous Materials, 2013, 167, 198-206.	4.4	13
77	Growth of Fe-doped ZnO nanorods using aerosol-assisted chemical vapour deposition via in situ doping. Applied Physics A: Materials Science and Processing, 2014, 116, 1801-1811.	2.3	13
78	Facile Fabrication of rGO/Rutile TiO2 Nanowires as Photocatalyst for Cr(VI) Reduction. Materials Today: Proceedings, 2019, 17, 1143-1151.	1.8	13
79	Nanoporous anodic Nb2O5 with pore-in-pore structure formation and its application for the photoreduction of Cr(VI). Chemosphere, 2021, 283, 131231.	8.2	13
80	Optical properties of two-dimensional ZnO nanosheets formed by hot-water treatment of Zn foils. Solid State Communications, 2013, 162, 43-47.	1.9	12
81	Enhanced dye-sensitized solar cells performance of ZnO nanorod arrays grown by low-temperature hydrothermal reaction. International Journal of Energy Research, 2013, 37, n/a-n/a.	4.5	12
82	Photocatalytic performance of freestanding tetragonal zirconia nanotubes formed in H ₂ O ₂ /NH ₄ F/ethylene glycol electrolyte by anodisation of zirconium. Nanotechnology, 2017, 28, 155604.	2.6	12
83	Effects of temperature and crucible height on the synthesis of 6H-SiC nanowires and nanoneedles. Journal of Alloys and Compounds, 2009, 481, 345-348.	5.5	11
84	Synthesis of Cobalt/Gold Bimetallic Particles with Porous Flake-Like Nanostructures and Their Magnetic Properties. Nanoscience and Nanotechnology Letters, 2012, 4, 687-692.	0.4	11
85	Growth Mechanism of Cubic-Silicon Carbide Nanowires. Journal of Nanomaterials, 2009, 2009, 1-5.	2.7	10
86	Growth of ZnO Nanorods on Stainless Steel Wire Using Chemical Vapour Deposition and Their Photocatalytic Activity. Scientific World Journal, The, 2014, 2014, 1-9.	2.1	10
87	A WO3Nanoporous-Nanorod Film Formed by Hydrothermal Growth of Nanorods on Anodized Nanoporous Substrate. Journal of the Electrochemical Society, 2015, 162, E148-E153.	2.9	10
88	Segmented nanoporous WO3 prepared via anodization and their photocatalytic properties. Journal of Materials Research, 2016, 31, 721-728.	2.6	10
89	Study of ITO Glass Electrode Modified with Iron Oxide Nanoparticles and Nafion for Glucose Biosensor Application. Procedia Chemistry, 2016, 19, 50-56.	0.7	10
90	Controlled facile fabrication of plasmonic enhanced Au-decorated ZnO nanowire arrays dye-sensitized solar cells. Materials Today Communications, 2017, 13, 354-358.	1.9	10

#	Article	IF	CITATIONS
91	Formation of grassy TiO2 nanotube thin film by anodisation in peroxide electrolyte for Cr(VI) removal under ultraviolet radiation. Nanotechnology, 2020, 31, 435605.	2.6	10
92	The formation of WO ₃ nanorods using the surfactant-assisted hydrothermal reaction. Journal of Experimental Nanoscience, 2014, 9, 9-16.	2.4	9
93	Interaction of graphene electrolyte gate field-effect transistor for detection of cortisol biomarker. AIP Conference Proceedings, 2018, , .	0.4	9
94	Anodised porous Nb2O5 for photoreduction of Cr(VI). Materials Today: Proceedings, 2019, 17, 1033-1039.	1.8	9
95	Facile Fabrication of Plasmonic Enhanced Noble-Metal-Decorated ZnO Nanowire Arrays for Dye-Sensitized Solar Cells. Journal of Nanoscience and Nanotechnology, 2020, 20, 359-366.	0.9	9
96	Effective vortex pinning in MgB2thin films. Superconductor Science and Technology, 2002, 15, 1392-1397.	3.5	8
97	Surface oxidation of cube-textured Ni–Cr for the formation of a NiO buffer layer for superconducting coated conductors. Physica C: Superconductivity and Its Applications, 2002, 383, 127-139.	1.2	8
98	Annealing temperature-dependent crystallinity and photocurrent response of anodic nanoporous iron oxide film. Journal of Materials Research, 2016, 31, 1681-1690.	2.6	8
99	Rapid TiO ₂ Nanotubes Formation in Aged Electrolyte and Their Application as Photocatalysts for Cr(VI) Reduction Under Visible Light. IEEE Nanotechnology Magazine, 2018, 17, 1106-1110.	2.0	8
100	Design and synthesis of mesoporous ZrO2 thin films using surfactant Pluronic P123 via sol-gel technique. Journal of the Ceramic Society of Japan, 2011, 119, 517-521.	1.1	7
101	Influence of post-deposition annealing on metal-organic decomposed lanthanum cerium oxide film. , 2011, , .		7
102	Zinc Oxide Nanostructures Formed by Wet Oxidation of Zn Foil. Advanced Materials Research, 0, 1043, 22-26.	0.3	7
103	Thermal oxidation of seeds for the hydrothermal growth of WO3 nanorods on ITO glass substrate. Thin Solid Films, 2015, 595, 73-78.	1.8	7
104	Effect of Fluoride or Chloride Ions on the Morphology of ZrO2 Thin Film Grown in Ethylene Glycol Electrolyte by Anodization. Procedia Chemistry, 2016, 19, 611-618.	0.7	7
105	Synthesis of TiO ₂ Nanotube Arrays in NaOH Added Ethylene Glycol Electrolyte and the Effect of Annealing Temperature on the Nanotube Arrays to their Photocurrent Performance. Key Engineering Materials, 2016, 701, 28-32.	0.4	7
106	Formation of anodic zirconia nanotubes in fluorinated ethylene glycol electrolyte with K 2 CO 3 addition. Surface and Coatings Technology, 2017, 320, 86-90.	4.8	7
107	Sensitive detection of Pb ions by square wave anodic stripping voltammetry by using iron oxide nanoparticles decorated zinc oxide nanorods modified electrode. Materials Chemistry and Physics, 2021, 273, 125148.	4.0	7
108	Effect of Dodecylbenzenesulfonic acid as a Surfactant on the Properties of Polyaniline/Graphene Nanocomposites. Materials Today: Proceedings, 2019, 17, 864-870.	1.8	6

#	Article	IF	CITATIONS
109	Surface-oxidation studies of cube-textured, pure nickel to form NiO as a potential YBa2Cu3O7â^'x-coated conductor buffer layer. Journal of Materials Research, 2003, 18, 327-337.	2.6	5
110	Formation of ZnO Nanorods via Seeded Growth Hydrothermal Reaction. Applied Mechanics and Materials, 2011, 83, 116-122.	0.2	5
111	Effects of applied voltage on the properties of anodic zirconia thin film on (100) silicon. Thin Solid Films, 2012, 522, 117-124.	1.8	5
112	Properties of Al-Doped ZnO Nanorods Synthesized Using Low Temperature Hydrothermal Method. Materials Science Forum, 2016, 846, 459-464.	0.3	5
113	Cr(VI) removal on visible light active TiO2 nanotube arrays. AIP Conference Proceedings, 2018, , .	0.4	5
114	Effect of Concentration and pH of PBS to the Electrocatalytic Performance of Enzymatic Glucose Biosensor. Solid State Phenomena, 0, 290, 193-198.	0.3	5
115	Formation of self-organized ZrO2–TiO2 and ZrTiO4–TiO2 nanotube arrays by anodization of Ti–40Zr foil for Cr(VI) removal. Journal of Materials Research and Technology, 2022, 19, 2991-3003.	5.8	5
116	Fabrication of YBCO thick films on Nd2CuO4 buffered Ni tapes by liquid phase epitaxy. Physica C: Superconductivity and Its Applications, 2002, 372-376, 742-746.	1.2	4
117	Effect of Anodisation Parameters on the Formation of Porous Anodic Oxide on Ti, Zr and W. IOP Conference Series: Materials Science and Engineering, 2011, 18, 052004.	0.6	4
118	Crystallization of TiO ₂ Nanotubes Arrays Grown by Anodization of Ti in Organic Electrolyte. Advanced Materials Research, 0, 620, 412-417.	0.3	4
119	Sensitive and selective chloroform sensor using Fe2O3 nanoparticle-decorated ZnO nanorods in an aqueous solution. Journal of Materials Science: Materials in Electronics, 2019, 30, 18990-19000.	2.2	4
120	Influence of substrate temperature on physical properties of CuAlO2 thin films grown via nitrate route pyrolytic reaction. Materials Science and Engineering B: Solid-State Materials for Advanced Technology, 2019, 240, 69-74.	3.5	4
121	Anodized TiO2 nanotubes using Ti wire in fluorinated ethylene glycol with air bubbles for removal of methylene blue dye. Journal of Applied Electrochemistry, 2022, 52, 173-188.	2.9	4
122	YBCO/Nd2CuO4/NiO/Ni coated conductors fabricated by liquid phase epitaxy based techniques. Superconductor Science and Technology, 2004, 17, 1144-1147.	3.5	3
123	Formation and Mechanistic Study of Self-Ordering ZrO ₂ Nanotubes by Anodic Oxidation. Advanced Materials Research, 2010, 173, 173-177.	0.3	3
124	Formation of Zirconia and Titania Nanotubes in Fluorine Contained Glycerol Electrochemical Bath. Defect and Diffusion Forum, 0, 312-315, 76-81.	0.4	3
125	Properties of ZnO Nanorods Arrays Growth via Low Temperature Hydrothermal Reaction. Advanced Materials Research, 0, 364, 422-426.	0.3	3
126	Formation of Anodic Oxide Nanotubes in H ₂ O ₂ - Fluoride Ethylene Glycol Electrolyte as Template for Electrodeposition of α-Fe ₂ O ₃ . Advanced Materials Research, 0, 832, 333-337.	0.3	3

#	Article	IF	CITATIONS
127	Formation of freestanding ZrO2 nanotubes for Cr(VI) removal. AIP Conference Proceedings, 2016, , .	0.4	3
128	Effect of NaOH Concentration on the Formation of TiO ₂ Nanotube Arrays by Anodic Oxidation Process for Photoelectrochemical Cell. Solid State Phenomena, 2017, 264, 152-155.	0.3	3
129	Synthesis colloidal Kyllinga brevifolia-mediated silver nanoparticles at different temperature for methylene blue removal. AIP Conference Proceedings, 2017, , .	0.4	3
130	Tailoring Parameters to Produce Nanowires on Metal Surface via Surface Oxidation Process. Journal of Physics: Conference Series, 2018, 1082, 012052.	0.4	3
131	Synthesis of TiO ₂ Nanotubes Decorated with Ag Nanoparticles (TNTs/AgNPs) For Visible Light Degradation of Methylene Blue. Journal of Physics: Conference Series, 2018, 1082, 012105.	0.4	3
132	Glucose-sensing properties of citrate-functionalized maghemite nanoparticle–modified indium tin oxide electrodes. Journal of Materials Research, 2020, 35, 1279-1289.	2.6	3
133	Metal oxide for heavy metal detection and removal. , 2020, , 299-332.		3
134	Formation of Dense and High-Aspect-Ratio Iron Oxide Nanowires by Water Vapor-Assisted Thermal Oxidation and Their Cr(VI) Adsorption Properties. ACS Omega, 2021, 6, 28203-28214.	3.5	3
135	Effect of postdeposition annealing on electrical properties of RFâ€magnetron sputtered CeO _{<i>x</i>} gate on 4Hâ€silicon carbide. Physica Status Solidi (A) Applications and Materials Science, 2011, 208, 1925-1930.	1.8	2
136	Tungsten Oxide Nanoporous Structure Synthesized Via Direct Electrochemical Anodization. , 2011, , .		2
137	Synthesis of au/co hollow microspheres via galvanic replacement reaction in organic solvent. World Journal of Engineering, 2012, 9, 493-500.	1.6	2
138	<i>Ex Situ</i> Doping of ZnO Nanorods by Spray Pyrolysis Technique. Materials Science Forum, 2013, 756, 16-23.	0.3	2
139	Preparation of WO ₃ Nanorods by Seeded Growth Hydrothermal Reaction. Advanced Materials Research, 0, 1024, 91-94.	0.3	2
140	Formation of Two-Dimensional ZnO Nanosheets by Rapid Thermal Oxidation in Oxygenated Environment. Journal of Nanoscience and Nanotechnology, 2014, 14, 2960-2967.	0.9	2
141	Photoelectrocatalytic activity of Zn-loaded RGO-TiO2composite coatings on mild steel substrate via DC electrochemical co-deposition. EPJ Applied Physics, 2014, 65, 20303.	0.7	2
142	Formation of Aligned Iron Oxide Nanopores as Cr Adsorbent Material. Advanced Materials Research, 2015, 1087, 460-464.	0.3	2
143	Effect of KOH added to ethylene glycol electrolyte on the self-organization of anodic ZrO2 nanotubes. AIP Conference Proceedings, 2016, , .	0.4	2
144	Kyllinga brevifolia mediated greener silver nanoparticles. AIP Conference Proceedings, 2017, , .	0.4	2

#	Article	IF	CITATIONS
145	Hierarchical Porous α-Fe ₂ O ₃ Formation by Thermal Oxidation of Iron as Catalyst for Cr(Vi) Reduction. Journal of Physics: Conference Series, 2018, 1082, 012044.	0.4	2
146	Hydrothermal growth of Fe2O3 nano/micro-rods on Fe foil for Cr(VI) removal. Materials Today: Proceedings, 2019, 17, 1018-1023.	1.8	2
147	Water Adsorption Characteristics and Microcalorimetric Studies of MOF-5 and MOF-199 Synthesized Using ``Green'' Sol-Gel. Acta Physica Polonica A, 2019, 135, 1119-1122.	0.5	2
148	Selective oxidation of cube textured Ni and Ni–Cr substrate for the formation of cube textured NiO as a component buffer layer for REBa2Cu3O7+x (REBCO) coated conductors. Physica C: Superconductivity and Its Applications, 2002, 372-376, 831-834.	1.2	1
149	Characterisation of MgB2 thin films of varying Tc by Raman spectroscopy. Journal of Physics and Chemistry of Solids, 2006, 67, 333-335.	4.0	1
150	CURRENT CONDUCTION MECHANISMS OF ATOMIC-LAYER-DEPOSITED Al2O3/NITRIDED SiO2 STACKING GATE OXIDE ON 4H-SiC. International Journal of Modern Physics B, 2010, 24, 5371-5378.	2.0	1
151	Protective Agent-Free Synthesis of Colloidal Cobalt Nanoparticles. , 2010, , .		1
152	Formation of 1-dimensional (1D) and 3-dimensional (3D) ZnO nanostructures by oxidation and chemical methods. Materialwissenschaft Und Werkstofftechnik, 2012, 43, 457-460.	0.9	1
153	Structural and Optical Properties of Fe-Doped ZnO Nanorods. Advanced Materials Research, 0, 858, 151-158.	0.3	1
154	Effects of Post-Deposition Annealing Time on Metal-Organic Decomposed Lanthanum Cerium Oxide Film Spin-Coated on Si Substrate. Advanced Materials Research, 0, 1024, 364-367.	0.3	1
155	Effect of Applied Voltage on the Formation of Self-Organized Iron Oxide Nanoporous Film in Organic Electrolyte via Anodic Oxidation Process and their Photocurrent Performance. Advanced Materials Research, 0, 1024, 99-103.	0.3	1
156	Properties of BaZr _x Ti _{1-x} O ₃ Thick Film Deposited Using EPD Method. Advanced Materials Research, 0, 1087, 465-469.	0.3	1
157	Formation of TiO2 nanotube arrays in KOH added fluoride-ethylene glycol (EG) electrolyte and its photoelectrochemical response. AIP Conference Proceedings, 2016, , .	0.4	1
158	Formation of TiO2 nanotube arrays by anodic oxidation in LiOH added ethylene glycol electrolyte and the effect of thermal annealing on the photoelectrochemical properties. AIP Conference Proceedings, 2016, , .	0.4	1
159	Effect of calcination temperature on the photodegradation efficiency of Ni/ZnO composite in removal of organic dye. AIP Conference Proceedings, 2017, , .	0.4	1
160	The effect of colloidal silica nanoparticles encapsulated fluorescein dye using micelle entrapment method. AIP Conference Proceedings, 2018, , .	0.4	1
161	Performance of zinc oxide particles as liquid ethanol sensor. Materials Today: Proceedings, 2019, 17, 976-981.	1.8	1
162	Oxide nanotubes formation by anodic process and their application in photochemical reactions for		1

² heavy metal removal. , 2020, , 277-303.

#	Article	IF	CITATIONS
163	Thermally oxidized steel mesh for oil-water separation application and its automation device. Environmental Nanotechnology, Monitoring and Management, 2021, 16, 100538.	2.9	1
164	Formation and photoelectrochemical properties of TiO2 nanotube arrays in fluorinated organic electrolyte. Journal of Mechanical Engineering and Sciences, 2017, 11, 3129-3136.	0.6	1
165	Photoreduction of Cr(VI) in wastewater by anodic nanoporous Nb2O5 formed at high anodizing voltage and electrolyte temperature. Environmental Science and Pollution Research, 2022, 29, 60600-60615.	5.3	1
166	Anodic film on Ti: Nanotubes formation and application for Cr(VI) and Cd(II) removal. Materials Today: Proceedings, 2022, , .	1.8	1
167	Study of the Surface Oxidation Epitaxy of Pure Ni. Materials Science Forum, 2003, 426-432, 3531-3536.	0.3	0
168	Synthesis of R-SiC nanowires via catalyst-free chemical vapour growth route. , 2008, , .		0
169	Oxidation of Copper for Copper Oxide Nanowires Production. , 2010, , .		Ο
170	Tungsten oxide nanoporous structure synthesized via direct electrochemical anodization. , 2010, , .		0
171	Study on Tungsten Oxide (WO ₃) Nanostructures Formation via Seeded Growth Hydrothermal Reaction. Applied Mechanics and Materials, 0, 83, 204-209.	0.2	Ο
172	Formation of CuAlO2Film by Ultrasonic Spray Pyrolysis. IOP Conference Series: Materials Science and Engineering, 2011, 18, 082022.	0.6	0
173	Effect of sputtering time on physical and electrical properties of ZrOxthin film on Si. Microelectronics International, 2011, 28, 7-11.	0.6	Ο
174	Structural and Optical Properties Thin Film Copper Oxides Formed by Chemical Solution Deposition Process Technique. , 2011, , .		0
175	Self Ordering of Anodic ZrO[sub 2] Nanotubes in Viscous Glycerol Electrolyte Using Anodization. , 2011, , .		Ο
176	Surface and Structural Properties of TiO ₂ Nanotubes Formation via Electrochemical Anodization. Advanced Materials Research, 0, 686, 71-76.	0.3	0
177	Electrolyte Influence on the Morphologies of Anodic ZrO ₂ Nanotube Arrays Formed by Anodization. Advanced Materials Research, 0, 1024, 104-107.	0.3	Ο
178	Effect of Annealing Temperature of Hybrid CeO ₂ /TiO ₂ Nanotubes on the Photocurrent. Advanced Materials Research, 0, 1024, 132-135.	0.3	0
179	The Effect of Crystallinity of Nanoporous WO ₃ on the Intercalation and Deintercalation of Li ⁺ . Advanced Materials Research, 0, 1024, 128-131.	0.3	0
180	Formation of raspberry like cobalt particles with hydrazine reduction in a polyol route. AIP Conference Proceedings, 2016, , .	0.4	0

#	Article	IF	CITATIONS
181	Anodic ZrO ₂ Nanotube Arrays Formation by Anodisation in Ethylene Glycol with Varying Amount of Water. Solid State Phenomena, 0, 264, 224-227.	0.3	Ο
182	Characterizations and photoelectrochemical properties of Fe2O3 and ZrO2 nanotubes formed by anodic oxidation process. AIP Conference Proceedings, 2017, , .	0.4	0
183	Formation of anodic TiO2 nanotube arrays in NaOH added fluoride-ethylene glycol electrolyte for dye-sensitized solar cells. AIP Conference Proceedings, 2017, , .	0.4	0
184	Morphology Controlled Synthesis of ZnO Nanorods for Glucose Enzymatic Biosensor. Solid State Phenomena, 0, 290, 280-285.	0.3	0
185	A-13 SOFT COMBUSTION SYNTHESIS OF NANOCRYSTALS SEMI-CONDUCTING TETRAGONAL ZIRCONIA POWDER(Session: Ceramics III). The Proceedings of the Asian Symposium on Materials and Processing, 2006, 2006, 13.	0.0	Ο
186	Thermal oxidation of steel mesh for water-oil separation process. Materials Today: Proceedings, 2022, 66, 2952-2956.	1.8	0